Tri-dimensional optical inspection based on flexible image guide: first step toward 3D industrial endoscopy

Erwan Dupont, Frédéric Lamarque, Christine Prelle, Tanneguy Redarce

TRI-DIMENSIONAL OPTICAL INSPECTION BASED ON FLEXIBLE IMAGE GUIDE: FIRST STEP TOWARD 3D INDUSTRIAL ENDOSCOPY

Erwan Dupont, Frédéric Lamarque, Christine Prelle
Université de Technologie de Compiègne
Laboratoire Roberval UMR 6253
Compiègne, France

Tanneguy Redarce
Institut National des Sciences Appliquées
Laboratoire Ampère UMR 5005
Lyon, France

ABSTRACT

3D optical endoscopy is now a major challenge to allow the high resolution inspection of industrial equipments. The proposed instrument is based on a flexible image guide (70 000 fibres) and a Digital Micro mirror Device (DMD, 1024 x 768 "on-off" micro mirrors). The optical design is as follows: the light emitted by a 532 nm laser diode is dynamically structured by the DMD chip as a fringes pattern which is phase-shifted due to the active control of the DMD chip and projected onto an object on a circular field of 6 mm in diameter. Due to a telecentric and binocular arrangement that creates a stereoscopic angle, it is possible to get a depth of field of 2 mm along the optical axis without keystone distortions and few disturbances created by defocus and coma aberrations. Then, images are captured by a 1024 x 768 digital camera (not yet moved away by fibres) at 15 fps and directly used in the reconstruction algorithm to access the tri-dimensional shape of the unpainted object. The results are compared to incoherent white light results obtained with white painted mechanical objects. The lateral resolution is 31.3 µm and the RMS axial resolution is 10 µm for the laser-based design after speckle attenuation.

INTRODUCTION

Nowadays, tri-dimensional inspection of mechanical systems (turbines, over-pressured industrial equipments, etc) and structures (bridges, buildings, etc) is mostly done by ultrasound techniques which present two majors drawbacks: the resolution is limited by the wavelength and due to the measurement probes size, intra-tubular inspection is quite difficult. To overcome these drawbacks, several methods have been explored to provide tri-dimensional measurements in an optical endoscopic context.

Active stereovision using diffracted structured light (dot matrix) injected into a fibre optic was demonstrated over objects with known geometries (1). Some studies describe a more complex instrumentation such as the spectrally encoded method (2) or the endoscopy based on the scanning of the illumination fibre over the object (3). In this last case, it is necessary to use multiple photodiodes to access the tri-dimensional shape of the object. These two last methods need complex photo-detectors such as spectrometer or sensors array. In the case of active stereovision, the photodetectors are simpler but this method requires precise fabricated diffraction gratings (4-7). Another strategy is to do the projection of interferograms created by muti-core fibre-based instruments (8, 9).

Fringe projection methods are interesting to get the 3D shape of the illuminated objects by analyzing the phase shift of the fringes. Albertazzi et al made the choice to design a special helical fringe projector which was composed of printed helical lines onto the inner surfaces of a cylinder illuminated by a central lamp (10). However, this strategy remains less flexible than the one based on the integration of a DLP (Digital Light Processing technology) projector or on the set "DMD (Digital Micro-mirror) chip + controller" in the measurement principle. Several studies have demonstrated the interest of this technology for high resolution (11), and high-speed (12) 3D shape measurements. Moreover, this technology brings flexibility to generate complex coding strategies for the structured light compared to fixed diffraction-based fringe patterns (13). Fringes projection generated by DLP projector and injected into image guide were

adapted to a stereomicroscope (14) and a miniaturized profilometer having a small probe (15).

In our previous work we have demonstrated it was possible to avoid keystone aberrations in a telecentric and binocular optical design (16) coupled with a DMD chip and its controller. In this work, we propose the integration of a 1.2 mm in diameter image guide in the projection channel while keeping a telecentric and binocular optical design. Moreover, a laser source (532 nm) for which the speckle was strongly reduced is tested and allows the 3D measurements at 15 fps of small details over unpainted metallic and specular mechanical parts.

INSTRUMENTAL DESCRIPTION

The figure 1 describes the whole optical system that is used to capture a 3D shape. The main property of this system is its binocular layout. It's consequently made up of 2 channels, the first one for the projection and based on a Digital Micro-mirror Device chip (DMD) and the second one for the acquisition and based on a CCD sensor. A 55 degrees stereoscopic angle between these two channels encodes the depth information. One other feature of this instrument is the use of an image guide in the projection channel. This image guide consequently put the projection part of the system away from the measurement zone.

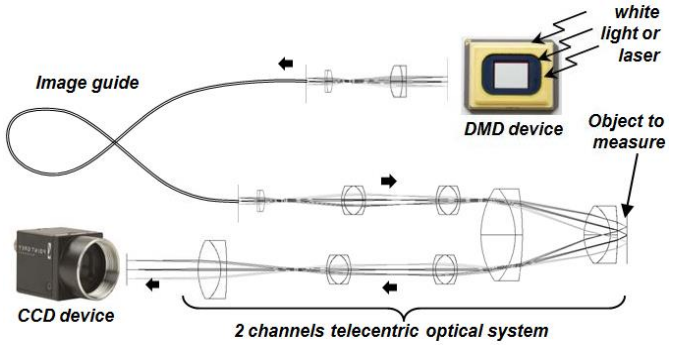

FIGURE 1 – Optical system description

The DMD chip is made of 1024x768 micro mirrors of 10.8 µm pitch. Each mirror on this device can be tilted between two orientations over a range of ± 12°. In one of the two orientations, the incident light (incoherent white light or laser) is aligned with the optical system whereas, for the other orientation, light is out of the system. This allows the projection of a high variety of patterns at high rates (higher than camera frame rate), which is interesting in case of phase shifting projection methods where the phase of the signal can be shifted at small time increments.

The image guide is composed of 70 000 optical cores that enables an image to be transmitted from the first end to the other. The diameter of this image guide is of 1.2 mm and its length is of 2 meters. The use of the image guide in this experimental setup is the first step towards the miniaturization of the 3D measurement system.

The CCD sensor records images of 1024x768 pixels for which a pixel pitch is equal to 4.65 µm. Each parameter of this CCD sensor such as contrast, luminosity and shutter delay can be finely tuned and its maximum frame rate is 30 images per second. Consequently because the DMD chip maximum frequency is much higher than 30 Hz, the acquisition of the fringe patterns can be made at the maximum CCD sensor frequency.

Each optical channel is composed of 5 achromatic lenses where two of them are common for both the channels (figure 1). The choice of achromatic lenses allows reducing both the chromatic and geometrical aberrations throughout the optical system. The two common lenses (placed at the final end of the optical system, near the object to measure) are entered by the light out of their principal axis. This out-of-axis configuration creates the stereoscopic angle and is a convenient way to reduce the size of the stereovision system. A possible drawback of this kind of out-of-axis entrance configuration is to increase the amount of distortion and diverse aberrations such as field curvature, astigmatism, coma… To overcome these potential various distortions effects, an optical optimization based on a custom merit function was done with the optical software Zemax EE. This optimization modifies the distance between the different lenses and/or the curvature radii and materials of the lenses in order to minimize distortion and aberration effects.

Another property of the proposed optical system is that the projection and acquisition channel are afocal. Therefore, parallel light coming from the image guide will exit the closer lens to the measured object with parallel rays and parallel light coming from the object will also reach the CCD sensor parallel. There are two advantages of this type of design. The first one is that the size of the fringe pattern projected onto the object remains unchanged whatever the position considered along the optical axis. Secondly, the size of the image of the object captured by the CCD sensor will also remain unchanged along the optical axis. These two advantages make simpler the 3D reconstruction because no keystone aberrations take place.

The proposed instrument can measure on a 6mm diameter field of view and 2mm depth of field. To highly increase the size of the measured 3D shape of the objet, it is possible to merge several adjacent 3D capture of the object. In another study (17) the mapping of several 2D adjacent endoscopic images onto 3D ultrasound model of the same object is proposed. In this study, the spatial coordinates of the endoscopic images and the ultrasound images are first acquired by a 3D position tracking device. Then, a mapping algorithm merges the two kinds of images to render an expended 3D shape of the object in which the measured resolution is preserved.

In case of the laser light use, a specific set-up was built to strongly reduce the speckle effect. Indeed, this effect has a direct influence over the lateral and axial resolutions because bright as well as dark fringes are no more homogeneous. The laser light emitted by a 532 nm wavelength laser diode was injected into a 2 meters long multimode optical fibre (emitting core diameter = 400 µm, NA = 0,39). After this, a part of the fibre was fixed onto a B&K mini-shaker 4810 powered by a 2718 B&K amplifier. This amplifier was driven by a function generator which applies a sinusoidal signal at 400 Hz frequency. With this set-up, a line pair of bright and dark fringes having a width of 62.6 µm onto the object (31.3 µm for each fringe corresponding to 3 pixels of the DMD chip) was well contrasted.

THE PHASE SHIFT BASED ALGORITHM

The reconstruction algorithm used to get the 3D shape of the illuminated object is based on a phase shift algorithm. This algorithm is rather developed for high precision measurements than optimized for fast computations. The principle of this reconstruction algorithm is composed of four steps (figure 2).

Vertical binary lines are projected onto the measured object and are shifted horizontally pixel per pixel. For each CCD sensor pixel, the intensity function is captured. The phase value of this intensity function, measured on the step two of the global 3D reconstruction method (figure 2), is applied on the step three and four of this method to obtain the final height information.

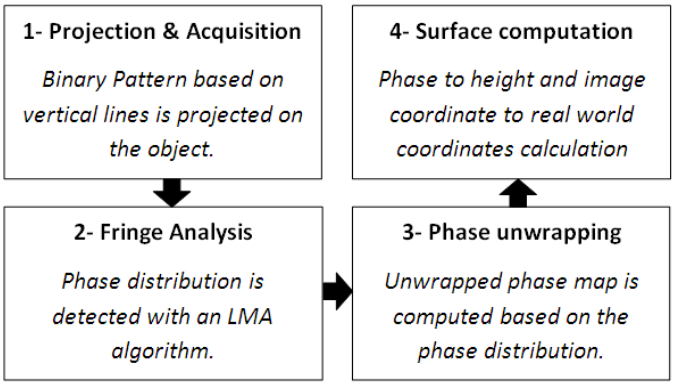

FIGURE 2 – global 3D-Reconstruction method

As stated above, the signal captured by each pixel of the CCD sensor can be represented with an intensity function. This intensity function F(t) is represented in figure 3 and is calculated with the convolution of the binary projected pattern function G(t) and the blurred effect function H(t) as shown in equation 1.

$$F(t) = G(t) * H(t) \tag{1}$$

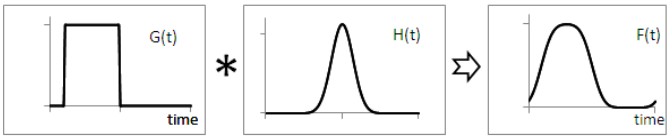

FIGURE 3 – Calculation of the captured signal F(t)

The G(t) function given in equation 2, represent the binary pattern projected from one pixel of the DMD to the object (u(t) is the step function).

$$G(t) = u(t - t_0) - u(t - t_1) \tag{2}$$

The duty cycle of the binary projected pattern can be determined by the t_0 and t_1 parameters. In highly blurred measurement condition, a small duty cycle can ease the detection of the illuminated part of the pattern by avoiding overlap in the bright parts of the pattern. In low blurred condition, a 50% duty cycle with a low period of detection is optimal.

The function H(t) is equivalent to the blurred effect due to the various distortions and diffraction effect in the optical system (Eq.(3)).

$$H(t) = \frac{1}{\sigma\sqrt{\pi}} exp\left(-\left(\frac{x}{\sigma}\right)^2\right) \tag{3}$$

The blurred effect in the measurement is fixed by the σ parameter. This standard deviation can be evaluated with the point spread function (PSF) of the whole measurement optical system (projection and acquisition parts). The PSF of the system was approximated to a 2D circular Gaussian function and the value of the standard deviation σ was extracted from this Gaussian function.

The final expression of F(t) comes from the derivative of F(t) described in equation 4.

$$\begin{aligned} F'(t) &= (\delta(t - t_0) - \delta(t - t_1)) * H(t) \\ F'(t) &= H(t - t_0) - H(t - t_1) \end{aligned} \tag{4}$$

Where (δ(t) is the impulse function.

Finally, the primitive of F'(t) is obtained (Eqt. 5). It depends of the cumulative distribution function (cdf).

$$F(t) = \frac{1}{2} cdf\left(\frac{t - t_0}{\sigma}\right) - \frac{1}{2} cdf\left(\frac{t - t_1}{\sigma}\right) \tag{5}$$

The final identification of a measured signal of 1 pixel of the CCD sensor will depend on 3 parameters P_0, P_1 and P_2 (Eq (6)).

$$\begin{aligned} F(t, P) = \frac{P_1}{2} . [cdf\left(\frac{(t - t_0 - P_0)}{\sigma}\right) \\ - cdf\left(\frac{(t - t_1 - P_0)}{\sigma}\right)] + P_2 \end{aligned} \tag{6}$$

The P_0 parameter is the phase parameter needed for the 3D reconstruction algorithm. The P_1 parameter measures the intensity of the light coming to the CCD sensor. The P_2 parameter is the median intensity of the acquired pattern.

The Levenberg-Marquardt Algorithm (LMA) is applied to the function F to determine the three parameters values. To avoid false local minimization, these three parameters are initialized with approximate values (Eq.(7)). For one measured signal, the minimum and maximum values of the signal and the date T_{max} of the first maximum are detected.

$$P_0 = T_{max} \; ; \; P1 = max - min \; ; \; P2 = min \tag{7}$$

To apply the LMA, we use these notations:

$$\begin{aligned} F_1(x) &= \frac{1}{2} cdf(x) \qquad F_2(X) = \frac{1}{\sigma\sqrt{\pi}} exp\left(-\left(\frac{x}{\sigma}\right)^2\right) \\ T_0 &= (t - P_0 - t_0) \qquad T_1 = (t - P_0 - t_1) \end{aligned} \tag{8}$$

The gradient (Eq.(9)) is calculated with respect to the 3 parameters P_0, P_1, P_2.

$$\frac{\partial F(t,P)}{\partial P_0} = -P_1.[F_2(T_0) - F_2(T_1)]$$

$$\frac{\partial F(t,P)}{\partial P_1} = F_1(T_0) - F_1(T_1) \qquad (9)$$

$$\frac{\partial F(t,P)}{\partial P_2} = 1$$

The LMA gives the 3 estimated values of P_0, P_1 and P_2 and then the estimated value of P_0 is used in a phase unwrapping algorithm (figure 2). Considering the calibration of the experimental system, the 3D real world coordinates of one object point are computed. That object point is the one that was optically conjugated with the CCD pixel where the intensity function F(t) was measured.

EXPERIMENTAL RESULTS

Firstly, the Modulation Transfer Function (MTF) of the whole optical system was measured to get the value of the lateral resolution. To acquire and compute this MTF, fringe patterns of different width were projected onto a flat screen by the help of the DMD chip and the images of this projected pattern were captured by the CCD sensor. For each capture at various line widths, the contrast value was calculated between the dark and the bright fringes.

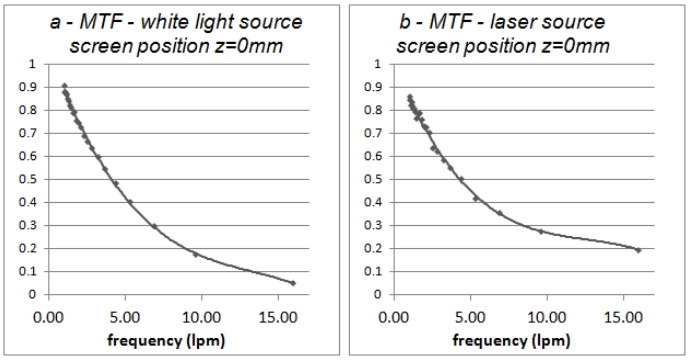

FIGURE 4 – Modulation transfer Function on a white flat surface

As seen in figure 4, the MTF done with the white light source and with the laser source are seemingly the same between 0 and 5 lpm (line pairs per millimeter). At low frequency it's rather the optical system than the light source that has a real impact on the MTF. However, when the frequency get higher than this 5 lpm limit, the MTF made with a white light source tend to the zero value at high frequency whereas the MTF made with a laser source tend to more than 0.1 value. This is due to the speckle projected by the laser source on the object that generates this higher contrast value than the one expected at these frequencies.

To estimate the lateral resolution, we looked for the highest line pair frequency the FFT can detect. The 16 lpm value is measured as the last detected frequency (figure 5) and this detection is validated for both white light source and laser source. So the lateral resolution is obtain at a frequency of 16 lpm, equivalent of a line width of 31.3 µm. It can be observe that the lateral resolution is obtained with low contrast fringe patterns which indicate the quality of the two optical channels.

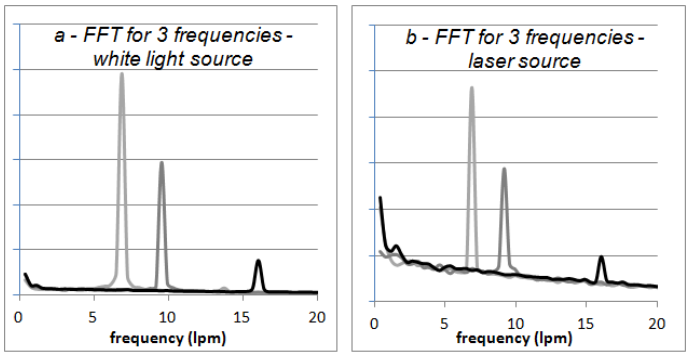

FIGURE 5 – FFT for 3 pattern frequencies

The MTF in figure 4 is not only a way to measure the lateral resolution but also a way to optimize the pattern frequency to be used in the 3D measurement process. To be sure that the projected pattern was robust and detected with various measurement conditions, the projected pattern frequency for the surface measurement process was fixed at a low value. The choice was made to use 32 pixels of the DMD chip per line pairs, which was equivalent to a 3 lpm frequency fringe pattern onto the projected flat screen. At this frequency, the contrast ratio is better than 0.6 over a normalized range. Consequently this projected pattern will be easily detected by the reconstruction algorithm.

To estimate the axial resolution, a white flat homogeneous screen was first placed in the measurement area of the experimental system. Then the shape of this screen was reconstructed with the process described in figure 2. Finally the depth value was stored for five different positions along the optical axis (figure 6).

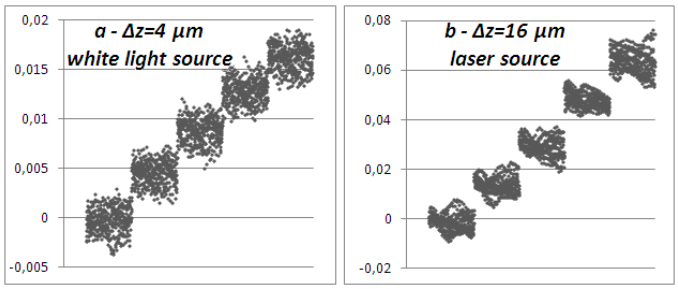

Figure 6 – white flat screen surface measurement with five axial shifts

The shift increment with a white light source was 4 µm and this shift became 16 µm in the case of a laser illumination. Both the incremental values were detected. It can be observed that the limit of resolution is reach for white light illumination whereas

it is lower than 16 µm for the laser. For this illumination mode, smaller steps down to 10 µm were detected as the limit.

After measuring the axial and lateral resolutions as well as the pattern fringe width, a 10 cents euro coin was measured in various conditions. The measurement of this coin was done for both illumination modes (white light and laser). In addition, the measurement was done when the coin was painted with a white diffuse paint or when it was not painted.

A surface reconstruction is presented in figure 7. This coin surface reconstruction was done in the best condition possible, namely with white paint on the coin and a white light source. All the various details of this 10 cents euro coin are easily detected.

Figure 7 – 3D surface reconstruction of the white painted 10 cents euro coin and with a white light source

Then a depth map of this ten cents euro coin in the four different conditions described above was acquired (figure 8). By looking this depth map, it can be seen that the measurement with white light illumination is smoother than the one with the laser one because the speckle adds noise to the result, despite its reduction with the method described in the instrumental part of this paper. However, using a laser source is a good way to apply more lighting power on the object. As a consequence, the laser illumination allows a higher frame rate from the CCD sensor and so a faster speed for the capture.

The standard deviation was measured on the flat parts of the coin in the four measurement conditions over a range of 32 000 measurement points. The standard deviation was of 1.8 µm in the best case (white painted coin and white light source). When the coin was not painted, the standard deviation was increased to 3.9 µm.

In case of laser source illumination, the standard deviation was 6.3 µm when the coin was painted and increased to 9.5 µm when it was not. That confirms that the measurement based on laser source is noisier but remains valid if the resolution is not the only measurement criteria. Consequently, to obtain the best resolution it can be worth to paint the object that need to be measured. However when painting is not possible, the measurement can be done with the cost of a relatively lower resolution but a higher frame rate.

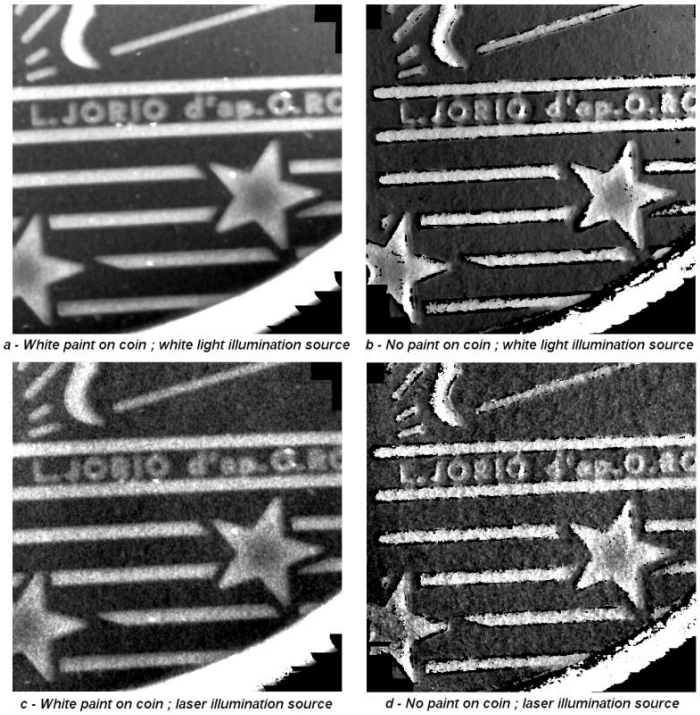

Figure 8 – Depth map of a coin with four measurement conditions

To get more precisions on the lateral and axial resolution, a 1D profile of the "J" and the "O" letters of the JORIO word inscribed on the surface of the coin were measured on the white painted coin illuminated by the white light source (figure 9 a) and with the laser source (figure 9 b). This choice of measurement was made because the words between the two parallel lines on the 10 cents euro coin are the smallest details that can be analyzed. To confirm the two 1D-profile described above, a measurement based on Zygo new view 200 with a magnification 2.5X was done (figure 10). The profile extracted with this interferometer represents the reference to check the validity of the results extracted by our stereoscopic instrument.

The lowest depth variation between the trough and the tops of the letter "J" is (25 ± 3) µm. This depth variation is easily detected on the two 1D-profile with white light or laser. The measure extracted from the profile obtained in figure 10 shows a mean depth value of (25.46 ± 1.00) µm. The agreement is very good for white light illumination as well as laser illumination. As expected, the 1D-profile made with the laser source is noisier, but regardless, the depth information can be extracted from this profile.

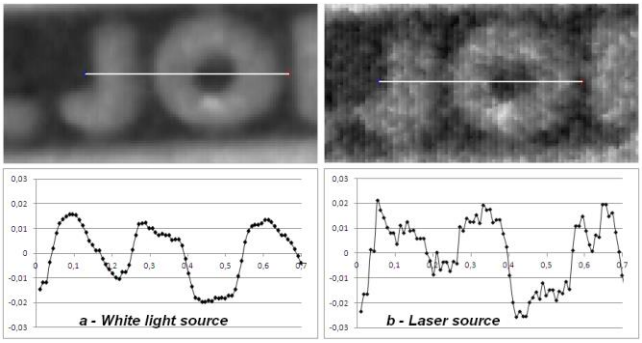

Figure 9 - Measured profile of the JO letters on the white painted 10 cents coin

To better confirm the depth resolution, a profile of the hole in the middle of the superior zone of the letter "R" was measured with the Zygo interferometer with a 10X magnification (figure 10). The measured height was (9,6 ± 0,5). It is obvious that the hole can be detected in figure 8 for the four measured depth maps. This confirms that the axial resolution of the measurement with or without painting in the both modes of illumination is lower or close to 10 µm.

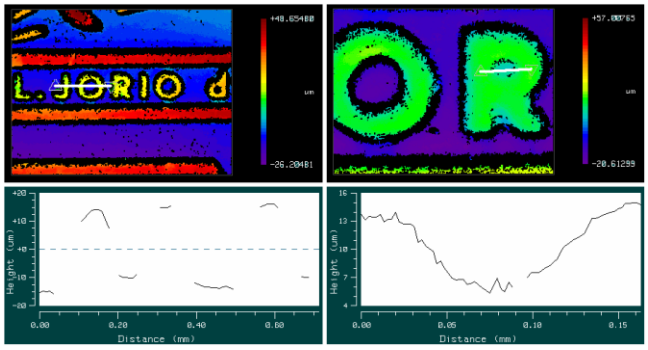

Figure 10 – Two measured profiles on the ten cents euro coin with a white light interferometer

A measurement was finally done on a black leather skin (figure 11) to confirm that the stereoscopic instrument can measure other type of materials than metallic ones. Even though the leather skin was of black texture, the measurement of the surface shape was possible. As stated above, the quality of the result is smoother with white light, but possible with laser light and measurement with laser light allow faster measurement time because laser can easier provide high light intensity on the object to measure. The results are quite similar to the real picture of the object already published in (16).

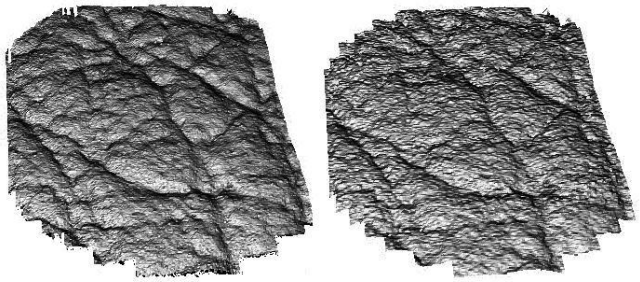

Figure 11 – shape measurement of black leather skin

CONCLUSION

An instrument based on a flexible image guide and a Digital Micro mirrors chip was described. It is able to measure a 3D shape of an object over a 6 mm diameter surface and a depth of field of 2 mm thanks to the phase-shift of a fringe pattern projected onto the illuminated object. The optical design includes a 532 nm laser diode that provides high optical power onto the illuminated object. This high brightness illumination mode allows a 15 fps frame rate measurement when the 3D shape of unpainted metallic or leather-based materials is reconstructed. Keystone distortions are avoided due to a symmetrical telecentric and binocular optical system that creates the stereoscopic angle.

In the worse case, the lateral resolution is 31.3 µm and the RMS axial resolution is 10 µm for the laser-based design after speckle attenuation. 1D-profiles are demonstrated over unpainted metallic coin and compared to white light interferometric measurements. Moreover, the instrument is able to provide the texture of an unpainted dark leather skin.

Future works will be to change the laser emitter for a Super Luminescent Diode (SLD), to move away the CCD sensor by the use of a second image guide and to design a miniaturized probe in order to permit 3D measurements in an endoscopic context.

REFERENCES

[1] Chan M., Lin W., Zhou C., Qu J., "Miniaturized three-dimensional endoscopic imaging system based on active stereovision", *Applied optics*, Vol 42, Issue 10, pp. 1888-1898, 2003

[2] Yelin D., White W.M., Motz J. T., Yun S.H., Bouma B. E., Tearney G. J., "Spectral Domain spectrally-encoded endoscopy" Optics Express, Vol. 15, Issue 5, pp. 2432-2444, 2008

[3] Smithwick Q. Y., Seibel E. J., "Depth enhancement using a scanning fiber optical endoscope", Proceedings of SPIE BiOS, Vol 4613, pp. 222 2333, 2002

[4] Iwata K.; Kusunoki F.; Moriwaki K.; Fukuda H., Tomii T., "Three-dimensional profiling using the Fourier transform method with a hexagonal grating projection", Applied optics, Vol. 47, Issue 12, pp. 2103-2108, 2008

[5] Su W., Reichard K., Yin S., Yu F.T.S., "Fabrication of digital sinusoidal gratings and precisely controlled diffusive flats and their application to highly accurate projected fringe profilometry", Optical Engineering, Vol. 42, (6), pp. 1730-1740, 2003

[6] Zhang J., Zhou C., Wang X., "Three-dimensional profilometry using a Dammann grating", Applied optics, Vol 48, Issue 19, pp. 3709-3715, 2009

[7] Spagnolo G. S., Ambrosini D., "Diffractive optical element-based profilometer for surface inspection", Optical Engineering, Vol 40, (1), pp. 44-52, 2001

[8] Bulut K., Inci M. N., "Three-dimensional optical profilometry using a four-core optical fibre", Optics & Laser Technology, Vol. 37, (6), pp. 463-469, 2005

[9] Yuan L., Yang J., Guan C., Dai Q., Tian F., "Three-core fiber-based shape-sensing application", Optics letters, Vol. 33, (6); pp. 578-580, 2008

[10] Albertazzi Jr. A. G., Hofmann A. C., Fantin A. V., Santos J. M. C. "Photogrammetric endoscope for measurement of inner

cylindrical surfaces using fringe projection", Applied Optics, Vol. 47, Issue 21, pp. 3868-3876, 2008

[11] Tsai M., Hung C., "Development of a high-precision surface metrology system using structured light projection", Measurement, Vol. 38, pp. 236-247, 2005

[12] Huang P., Zhang C., Chiang, F., "High-speed 3-D shape measurement based on digital fringe projection", Optical Engineering, Vol. 42, (1), pp. 163-168, 2003

[13] Salvi J., Pages J., Batlle J., "Pattern codification strategies in structured light systems", Pattern Recognition, Vol. 37, (4), pp. 827-849, 2004

[14] Fan K.; Li R., Song H., "Fibre image techniques in digital stereomicroscopy", Measurement Science and Technology, Vol. 17, pp. 373-378, 2006

[15] Chen L., Huang C., "Miniaturized 3D surface profilometer using digital fringe projection", Measurement Science and Technology, Vol 16, pp. 1061-1068, 2005

[16] Dupont E.; Lamarque F.; Prelle C., Redarce, T. "3D triangulation system based on out-of-axis aperture configuration for micro-scaled objects shape measurement", Proceedings of SPIE Photonic West, 7932, 79320F, doi: 10.1117 /12.874796, 2011

[17] Liao, H.; Tsuzuki, M.; Kobayashi, E. & Sakuma, I. "GPU-based Fast 3D Ultrasound-Endoscope Image Fusion for Complex-Shaped Objects", World Congress on Medical Physics and Biomedical Engineering, September 7-12, 2009, Munich, Germany, 2009, 206-209